Published in final edited form as:
*Nat Chem*. 2022 May ; 14(5): 566–573. doi:10.1038/s41557-022-00895-3.

# Stereocontrolled 1,3-nitrogen migration to access chiral α-amino acids

**Chen-Xi Ye**[#1], **Xiang Shen**[#1], **Shuming Chen**[2,*], **Eric Meggers**[1,*]

[1]Fachbereich Chemie, Philipps-Universität Marburg, Hans-Meerwein-Strasse 4, 35043 Marburg, Germany

[2]Department of Chemistry and Biochemistry, Oberlin College, Oberlin, Ohio 44074, United States

[#] These authors contributed equally to this work.

## Abstract

α-Amino acids are essential for life as building blocks of proteins and components of diverse natural molecules. In both industry and academia, the incorporation of unnatural amino acids is often desirable for modulating chemical, physical, and pharmaceutical properties. We here report a protocol for the economical and practical synthesis of optically active α-amino acids based on an unprecedented stereocontrolled 1,3-nitrogen shift. Our method employs abundant and easily accessible carboxylic acids as starting materials, which are first connected to a nitrogenation reagent, followed by a highly regio- and enantioselective ruthenium- or iron-catalyzed C($sp^3$)−H amination. This straightforward method displays a very broad scope, providing rapid access to optically active α-amino acids with aryl, allyl, propargyl, and alkyl side chains, and also permits stereocontrolled late-stage amination of carboxylic acid-containing drugs and natural products.



[*] shuming.chen@oberlin.edu and meggers@chemie.uni-marburg.de.

**Author contributions**

E.M. and S.C. wrote the manuscript. E.M. and C.-X.Y. conceived the project and devised the experiments for the Ru catalysis. E.M. and X.S. devised the experiments for the Fe catalysis. C.-X.Y. carried out the initial experiments and developed the ruthenium catalysis. X.S. developed the iron catalysis. S.C. performed the DFT calculations.

**Competing interests**

The authors declare no competing interests.

Europe PMC Funders Author Manuscripts

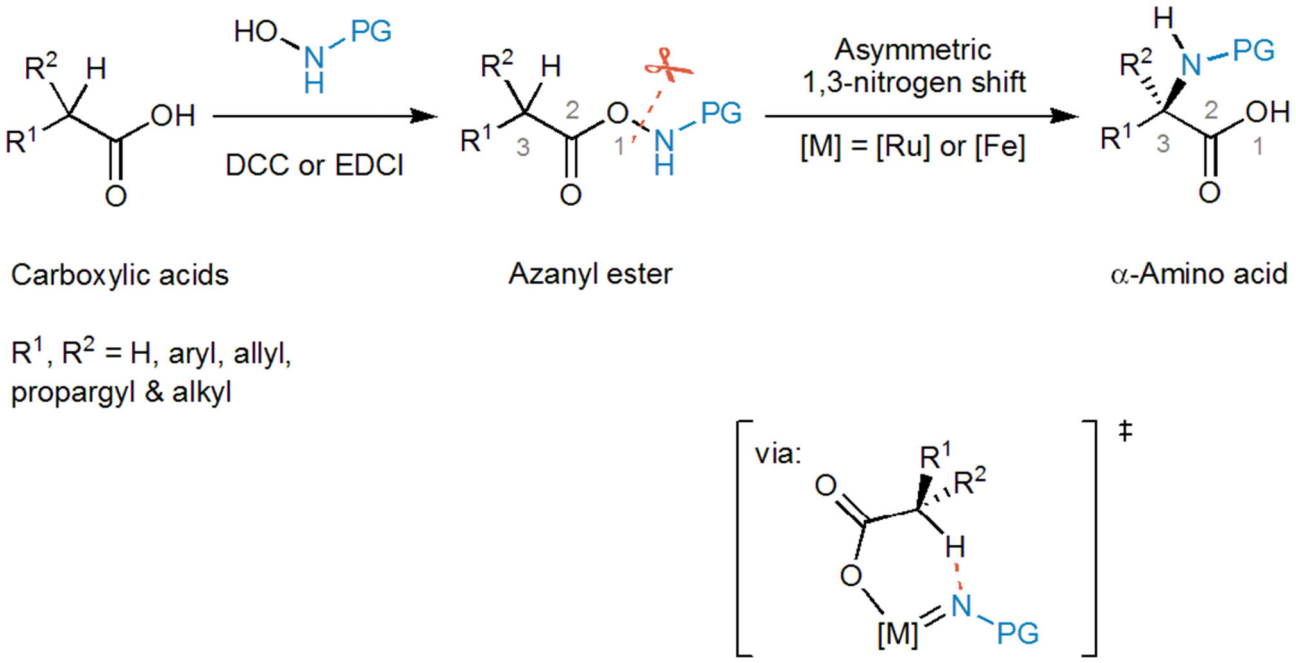


Summary of the article for the table of contents:
A straightforward method for synthesizing optically active α-amino acids from abundant carboxylic acids has been developed. The method features a nitrene-mediated stereocontrolled 1,3-nitrogen shift. It provides access to a large variety of unnatural α-amino acids with aryl, allyl, propargyl, alkyl side chains, and enables late-stage amination of carboxylic acid-containing drugs.

A direct and straightforward strategy for the synthesis of optically active α-amino acids is the catalytic enantioselective introduction of an amino group in α-position of readily available carboxylic acids.[1,2] A number of methods for direct asymmetric C($sp^3$)−H aminations have been reported and typically exploit the acidity of the C−H group next to a carbonyl functionality for electrophilic aminations via enolate intermediates.[3–7] However, most existing methods use aldehydes, ketones or dicarbonyl compounds as starting materials instead of more desirable but less acidic carboxylic acid derivatives. To further complicate matters, the electrophilic amination reagents employed are usually diazo compounds, which lead to amination products that cannot be easily converted to the target α-amino acids.

The insertion of nitrenes into C−H bonds provides a more tunable alternative platform for C($sp^3$)−H aminations as the reactivity of nitrenes can be controlled by transition metal coordination. In addition, milder reaction conditions can often be used (Figure 1a).[8] Much progress has been made employing chiral transition metal catalysts for the enantioselective conversion of prochiral C($sp^3$)−H bonds into C-N bonds by nitrene insertion.[9,10] However, intermolecular nitrene insertion reactions suffer from problems with

regioselectivity and enantioselectivity (Figure 1b).[11–19] Although this is not the case for intramolecular C($sp^3$)−H amination reactions, in which well-defined cyclic transition states allow exquisite regio- and stereocontrol, such intramolecular C−H nitrene insertions are typically ring-closing reactions and therefore lack general applicability.[20–26] Thus, the catalytic enantioselective synthesis of acyclic amines by catalytic enantioselective C($sp^3$)−H nitrene insertion remains a challenge, and its application to the synthesis of chiral α-amino acids would be highly desirable.

We here introduce a strategy that combines the advantages of intramolecular (regio- and stereocontrol via cyclic transition state) and intermolecular C−H nitrene insertion chemistry (more general, acyclic products) by covalently connecting a nitrene precursor to a carboxylic acid functionality. After O−N bond cleavage and binding of both fragments to the catalyst, a cyclic transition state facilitates a stereocontrolled C($sp^3$)−H amination (Figure 1c). This reaction constitutes an unprecedented stereocontrolled 1,3-nitrogen shift and is applied to the catalytic asymmetric synthesis of α-amino acids.

## Results and discussion

### Initial experiments and optimization

We commenced our study with carboxylic acid derivatives **1a**-**e** in which the nitrogen bears different electron-withdrawing protecting groups, which is established to be beneficial for generating electrophilic nitrene intermediates. The catalysts tested were “chiral-at-metal” ruthenium complexes in which two bidentate *N*-(2-pyridyl)-substituted *N*-heterocyclic carbenes and two acetonitrile ligands are coordinated to a central ruthenium in a $C_2$-symmetric fashion (Table 1).[27] Despite all ligands being achiral, the overall chirality required for asymmetric catalysis originates from a stereogenic ruthenium center with Λ or Δ configuration, resulting in a left-handed or right-handed helical topology, respectively. We have previously demonstrated such complexes to be capable of catalyzing enantioselective ring-closing C−H aminations.[28,29] Importantly, this class of catalysts feature two vacant coordination sites adjacent to each other (coordination sites of the two labile acetonitrile, highlighted in red), which is essential for the envisioned mechanistic design.

We first subjected the trifluoroacetamide substrate **1a** to the ruthenium complex **RuDMP**[27] (1 mol%) in $CH_2Cl_2$ in the presence of the base $K_2CO_3$ (3 equiv.) at room temperature (25 °C) for 16 hours, but were disappointed that no conversion occurred (Table 1, entry 1). Upon replacement of the trifluoroacetamide group with a *p*-toluenesulfonyl (Ts) group (**1b**), a 37% conversion was observed, although the undesired phenylacetic acid (**PAA**) was obtained as the main product in 23% yield as measured by $^1$H NMR (entry 2). Encouragingly, the amination product **2b** was also detected, albeit only in small quantities (<5%). A methylsulfonyl (Ms) group did not provide significantly better results with product **2c** formed in trace amounts (<5%) (entry 3). Because of the difficulties associated with cleaving sulfonylamides, sulfonyl groups are synthetically undesirable as amine protecting groups. We therefore tested the more practical methoxycarbonyl protecting group and were delighted to find that the substrate **1d** was completely consumed under our standard conditions and the chiral amino acid (*R*)-**2d** formed in 86% yield with 89% enantiomeric excess (e.e.) (entry 4). Finally, the best results were obtained with

the 2,2,2-trichloroethoxycarbonyl (Troc) protecting group (**1e**), which provided the amino acid (*R*)-**2e** in an excellent 93% yield as determined by $^1$H NMR and with 95% e.e. (entry 5). Other catalysts with different substituents on the pyridine moieties provided inferior results; replacing the 3,5-dimethylphenyl groups with trimethylsilyl (TMS) groups (**RuTMS**[28]), CF3 groups (**RuCF3$_3$**[29]), or just hydrogen (**RuH**[27]) resulted in reduced yields and enantioselectivities (entries 6-8). Table 1 also reveals that $CH_2Cl_2$ is the optimal solvent and $K_2CO_3$ the optimal base for this stereocontrolled 1,3-nitrogen shift (entries 9-12 and Supplementary Table 1).

## Substrate scope for ruthenium catalysis

With the optimal reaction conditions in hand, we investigated the scope of this stereocontrolled 1,3-nitrogen shift. *N,N'*-Dicyclohexylcarbodiimide (DCC)- or 1-ethyl-3-(3-dimethylaminopropyl)carbodiimide hydrochloride (EDCI)-induced coupling of readily available carboxylic acids with *N*-Troc-protected hydroxylamine provided rapid access to a variety of azanyl esters, which were then subjected to the rearrangement under the developed standard conditions (Table 2). We started with functionalizing the phenyl moiety of phenylacetic acid azanyl ester **1e** and found that the method tolerates a large variety of different substituents in the phenyl ring, affording the corresponding chiral α-amino acids **3**-**21** in up to 96% yield and with up to 98% e.e.. Electron-donating functional groups in the phenyl moiety such as methyl (α-amino acid **3**), methoxy (α-amino acids **5**), 1,3-dioxole (α-amino acid **8**), a Fmoc-protected alcohol (α-amino acid **9**), hydroxymethyl (α-amino acid **10**), and *N*-pivaloylamide (α-amino acid **19**) are tolerated, as are electron-withdrawing substituents such as halogens (α-amino acid **11**-**14**), trifluoromethyl (α-amino acid **15**), nitro (α-amino acid **16**), acetyl (α-amino acid **17**), and methoxycarbonyl (α-amino acid **18**). The method also enables the synthesis of the azido α-amino acid **20** (95% yield and 97% e.e.) and the alkynyl α-amino acid **21** (88% yield, 94% e.e.), both of which are building blocks of interest for click chemistry (see Supplementary Table 2 regarding the configurational stability of the generated 30 stereocenter).[30] The stereocontrolled 1,3-nitrogen shift was also applied to the synthesis of α-aryl amino acids with benzannulated aromatic and heteroaromatic systems (α-amino acids **22**-**25**) in 77-92% yield and with 90-96% e.e.. Notably, the reaction could be readily scaled up to afford the naphthyl α-amino acid **23** in gram quantities with high yield (91%) and enantiopurity (95% e.e., increased to 99% e.e. after crystallization protocol, see Supplementary Figure 1). It is noteworthy that the stereocontrolled 1,3-nitrogen shift can also be applied to the late-stage functionalization of bioactive compounds. For example, isoxepac[31] is an arylacetic acid derivative with anti-inflammatory and analgesic activity, and the azanyl ester of which was converted to the corresponding α-amino acid **26** in 87% yield and with 98% e.e.. Diclofenac,[32] a pain medication for the treatment of inflammatory diseases, was converted into its azanyl ester and then rearranged to afford α-amino acid **27** in 54% yield and with 96% e.e., which is remarkable considering the presence of an unprotected and sterically hindered aniline moiety in the *ortho*-position.

We also investigated C−H aminations at non-benzylic positions, and the stereocontrolled 1,3-nitrogen shift can be applied to the asymmetric synthesis of chiral α-amino acids with alkenyl (**28**-**32**) and alkynyl (**34** and **35**) side chains, albeit with somewhat

reduced enantioselectivities (62-84% e.e.). Even the unusual Troc-protected 2-amino-(*E*)-3,5-hexadienoic acid (**33**) could be synthesized in 72% yield and with 81% e.e.. These results show that the stereocontrolled 1,3-nitrogen shift is applicable to benzylic, allylic, and propargylic C−H bonds. However, the application to completely non-activated aliphatic methylene groups provides inferior results, with the α-amino acid **36** obtained in merely 20% yield, albeit with a satisfactory 90% e.e..

Next, we investigated the asymmetric synthesis of α-disubstituted α-amino acids by amination of tertiary C−H bonds at a stereogenic carbon center. When we reacted racemic azanyl ester **37** under our standard conditions, the corresponding 2-amino-2-phenylpropanoic acid (*R*)-**38** was obtained in 71% yield but with a modest 48% e.e.. Since the azanyl ester is chiral, we expected high stereodiscrimination between enantiotopic C−H bonds. Indeed, the *S*-enantiomer (*S*)-**37** (99% e.e.) afforded the α-amino acid (*R*)-**38** smoothly in 91% yield and with 98% e.e. (matched substrate/catalyst combination) while the mirror-imaged substrate (*R*)-**37** reacted sluggishly, providing the α-amino acid (*S*)-**38** in 34% yield with 28% e.e. (mismatched substrate/catalyst combination). The stereospecific C−H amination of chiral non-racemic substrates is general and was applied to the synthesis of the α-disubstituted α-amino acids **39**-**42** in 25-86% yield and with 86-99% e.e.. For example, the azanyl ester of the nonsteroidal anti-inflammatory drug naproxen, which contains an (*S*)-configured stereocenter, was converted to the corresponding α-amino acid **39** in 86% yield and 99% e.e., with virtually complete stereoretention. The C−H amination is also applicable to completely nonactivated tertiary C($sp^3$)−H bonds, as demonstrated by α-amino acids **41** and **42**.

## Substrate scope for iron catalysis

To expand the substrate scope, we turned our attention to iron catalysis,[33] which has additional economic and environmental benefits. Iron-catalyzed C−H bond aminations through nitrenoid intermediates have been reported, including the (racemic) amination of non-activated aliphatic C($sp^3$)−H bonds.[34] We utilized the conversion of azanyl ester **1e** to the *N*-Troc-protected phenylglycine **2e** as the initial model reaction to identify a suitable iron catalyst (Table 3). The chiral-at-iron complex Δ-**Fe1**,[35] a lighter homolog of the chiral-at-ruthenium complexes used in this study, provided disappointing results with only trace amounts of product. We next investigated non-heme iron complexes with linear tetradentate N4-donor ligands coordinated in a *cis*-α-topological configuration. The overall helical topology is similar to the ruthenium catalysts, including the presence of two adjacent labile ligands. Using bis-pyridine complexes (*R*,*R*)-**Fe2** and (*R*,*R*)-**Fe3** featuring a rigid chiral 2,2'-bipyrrolidine backbone,[36,37] we obtained the desired amino acid (*S*)-**2e** in 91% and 75% yield, respectively, albeit with <20% e.e.. Fortunately, replacing the pyridyl moieties with *N*-methylbenzimidazole[38] (**BIP** ligand) and using labile chloride ligands instead of acetonitrile resulted in the air- and moisture-stable neutral complex (*R*,*R*)-[$FeCl_2$(**BIP**)] ((*R*,*R*)-**FeBIP**), which provided phenylglycine (*S*)-**2e** in 95% yield and with a satisfactory 91% e.e.. While the amination of benzylic (**2e**), allylic (**32**) and propargylic (**34**) positions cannot compete with the results obtained for ruthenium catalysis, we found that (*R*,*R*)-**FeBIP** is a superior catalyst for the generation of non-racemic α-amino acids with non-activating aliphatic side chains. Substrates with primary (**43**-**50**), secondary (**51**), and tertiary (**36**) aliphatic side

Europe PMC Funders Author Manuscripts

chains underwent amination in 48-75% yield and with 85-92% e.e.. The method is also suitable for the late-stage amination of more complex molecules. Azanyl ester formation followed by iron-catalyzed stereocontrolled 1,3-nitrogen shift converted lithocholic acid to amino acid **52** (77% yield, 23:1 d.r.). The iron-catalyzed protocol can also be used for the amination of tertiary C($sp^3$)−H bonds as shown for racemic ibuprofen, which was converted to amino acid **53** in 70% yield and with 85% e.e. in a stereoconvergent transformation.

## Mechanistic investigations

We performed density functional theory (DFT) calculations to elucidate the reaction mechanism and provide deeper insight (Figure 2a). Ruthenium catalyst **RuH** and the methylcarbamate substrate **1d** were used as the model system. Since the catalyst contains two adjacent labile MeCN ligands and the azanyl ester substrate several suitable coordination sites, it is reasonable to expect that the mechanism proceeds through an initial bidentate coordination. Indeed, the DFT calculations are consistent with this picture. Stepwise displacement of two labile acetonitrile ligands from the Ru center of **RuH** by substrate **1d** gives rise to intermediate **I**, which proceeds to the chelate coordination mode **II** with a modest 6.2 kcal/mol increase in free energy. The amide N−H bond in **II** is now sufficiently acidified to be deprotonated by a weak base such as trimethylamine, leading to the deprotonated chelate intermediate **III**. A subsequent N−O cleavage occurs through the cyclic transition state **TS-I** with a free energy barrier of 13.6 kcal/mol to yield Ru nitrene **IV** in an exergonic fashion. Although the singlet nitrene complex $^1$**IV** is calculated to be 2.3 kcal/mol more stable than the triplet nitrene complex $^3$**IV**, the C−H cleavage transition state **TS-II** is significantly lower in energy in the triplet state ($^3$**TS-II** vs. $^1$**TS-II**). This indicates the possibility of a Curtin-Hammett situation in which the presence of the late transition metal ruthenium enhances rapid singlet-triplet spin crossover,[39–41] followed by a preferred exergonic hydrogen atom transfer (HAT) from $^3$**IV** through the cyclic transition state $^3$**TS-II** to afford the diradical $^3$**V**. Facile intersystem crossing between intersecting singlet and triplet energy surfaces has also been implicated in other systems involving nitrenoid intermediates, such as Cu- and Ag-catalyzed olefin aziridinations[42] and C($sp^3$)−H amidations promoted by a Ru photocatalyst.[43] An experimentally determined kinetic isotope effect (KIE) value of $k_H/k_D$ = 2.9 indicates that this homolytic C−H cleavage occurs during the rate-determining step and is consistent with the calculated free energy barrier of 13.9 kcal for the hydrogen atom transfer step on the triplet energy surface. A radical mechanism is also supported by an observed $Z \rightarrow E$ alkene isomerization in an allylic C−H amination reaction (see Supplementary Figure 2 for these mechanistic experiments). Taken together, these computational and experimental results indicate that the dominant mechanistic C−H cleavage pathway involves triplet hydrogen atom transfer, not concerted singlet nitrene insertion. Calculated spin densities of the intermediate $^3$**V**, formed in the course of the hydrogen atom transfer, indicate that the single occupied molecular orbitals (SOMOs) are mostly located on the Ru center and the α-carbon of the coordinated substrate so that intermediate $^3$**V**is best represented as a triplet diradical (see framed structure of $^3$V in Figure 2a). Intermediate $^3$V undergoes a strongly exergonic radical recombination to form $^1$VI upon spin crossover to the singlet state through a minimum energy crossing point (MECP). Subsequent O-protonation and release of product**2d** then completes the catalytic cycle.

Our calculations also provide insight into the origins of stereocontrol in the 1,3-nitrogen shift. Figure 2b shows the geometries of the calculated cyclic transition state for the hydrogen atom transfer step involving the model substrate **1d** bearing a phenyl substituent. Non-covalent interaction (NCI) plots reveal that the transition state leading to the experimentally observed major product enantiomer, **$^3$TS-II-major-Ph**, is stabilized by a **π-π** stacking interaction between a pyridine ligand of the catalyst and the phenyl substituent on the substrate. This **π-π** stacking interaction is absent from the disfavored minor transition state **$^3$TS-II-minor-Ph**, which is 1.5 kcal/mol higher in energy than **$^3$TS-II-major-Ph**. To evaluate the effect of solvent, when implicit $CH_2Cl_2$ solvent was incorporated in the TS geometry optimizations (see Supplementary Information, Sections 8.4-8.6), the free energy difference was found to be 2.1 kcal/mol favoring **$^3$TS-II-major-Ph** consistent with the calculations in the gas phase. Following the stereoselective HAT, the resulting diradical **V** presumably undergoes spin crossover and recombination faster than C−C bond rotation, allowing the stereoselectivity of the HAT step to be preserved in the nitrogenated product. This is consistent with the C−H amination of chiral substrates such as (*S*)-**37**, in which the C−H bond is converted to a C-N bond under retention of configuration. Distortion-interaction analysis[44] performed on the two transition states indicates that the distortion energies are 1.4 kcal/mol lower for **$^3$TS-II-minor-Ph**, but the interaction energy is 2.9 kcal/mol more favorable in **$^3$TS-II-major-Ph** (Figure 2c). These results provide further support that stabilizing interactions such as **π-π** stacking contribute to the observed stereoselectivity in the formation of phenyl glycine derivative **2d**. However, our calculations confirm that stereodiscrimination can also be achieved in the absence of attractive **π-π** stacking interactions as demonstrated for a substrate bearing a *tert*-butyl instead of a phenyl side chain, which is consistent with the experimental results (e.g. formation of amino acid **36**). The transition state producing the major product enantiomer, **$^3$TS-II-major-$^t$Bu**, was calculated to be 1.3 kcal/mol more favorable than **$^3$TS-II-minor-$^t$Bu**. This result is in good agreement with the experimentally observed 90% e.e. value. In **3TS-II-minor-$^t$Bu**, the *tert*-butyl substituent on the pyridylketone substrate sterically clashes with the acyl Ru-nitrenoid fragment, creating destabilizing close contacts that are absent from **$^3$TS-II-major-$^t$Bu**. Such destabilizing close contacts are also absent from the transition states with the phenyl side chain. Taken together, these results support the conclusion that effective stereodiscrimination can either be achieved through **π-π** stacking (in the case of Ph side chain) or steric effects (in the case of $^t$Bu side chain), although contributions from additional attractive interactions, such as C−H-**π** interactions, cannot be ruled out in **$^3$TS-II-major-$^t$Bu**.[45–47]

A simplified mechanism based on the DFT calculations and control experiments discussed above is shown Figure 3. The azanyl ester substrate is first activated by N−O cleavage to provide intermediate **A** (corresponding to intermediate **IV** in Figure 2a) after deprotonation. A subsequent stereocontrolled hydrogen atom transfer then affords the diradical **B** (corresponding to intermediate **V** in Figure 2a), followed by a rapid radical rebound to yield the chelate complex **C** (corresponding to intermediate **VI** in Figure 2a). Protonation of the carboxylate induces product dissociation and concludes the catalytic cycle. The net result of the N−O bond fragmentation and subsequent stepwise C−H insertion is an asymmetric 1,3-nitrogen shift to provide non-racemic chiral α-amino acids.

## Conclusions

In conclusion, we report the catalytic enantioselective synthesis of chiral α-amino acids by nitrene C($sp^3$)−H insertion. The method is based on a unique stereocontrolled 1,3-nitrogen shift from one carboxylic acid oxygen to the α-carbon. Our method employs abundant and easily accessible carboxylic acids as starting materials. Ligation to a nitrene precursor, followed by intramolecular C−H cleavage through a cyclic transition state, ensures high regio- and stereocontrol in the synthesis of non-racemic chiral α-amino acids. Chiral ruthenium and iron catalysis jointly provide a very broad scope, enabling rapid access to optically active α-amino acids with aryl, allyl, propargyl (ruthenium catalysis), and non-activated alkyl (iron catalysis) side chains, including α-disubstituted amino acids by stereoretentive (ruthenium catalysis) or enantioconvergent (iron catalysis) C−H amination. The high functional group tolerance of this method also permits the enantioselective late-stage amination of carboxylic acid-containing drugs and natural products. The Troc-protected amino acids obtained through this protocol can be used directly in synthesis with the Troc group being selectively removable under mild conditions via a reductive Grob fragmentation.[48] This strategy will expedite the synthesis of unnatural α-amino acids, which are important building blocks of peptidomimetic drugs, as well as engineered proteins and enzymes with modulated properties.[49–51]

## Methods

### General

For the $^1$H NMR, $^{13}$C NMR spectra and HPLC traces of compounds in this Article, details of synthetic procedures, as well as details of the computational study, see the Supplementary Information.

### General procedure for ruthenium catalyzed 1,3-nitrogen shift

To a Schlenk tube was added the azanyl ester (1 equiv.), $K_2CO_3$ (3 equiv.) and the ruthenium catalyst (1-2 mol% of Λ-**RuDMP** or 2-10 mol% of Λ-**RuH**). The tube was evacuated and backfilled with $N_2$ for three times. Dichloromethane (*c* 0.05 M) was added, and the tube was sealed. The reaction mixture was stirred at room temperature (25 °C) for 16 hours. After completion, the reaction was quenched by a mixture of brine and hydrochloric acid, and subsequently extracted with EtOAc. The combined organic layer was dried and was concentrated under reduced pressure, and the residue was purified by column chromatography on silica gel using a mixture of EtOAc and *n*-hexane (with 0.1% trifluoroacetic acid as the additive) to obtain non-racemic α-amino acids **2**-**36** and **38**-**42**.

### General procedure for iron catalyzed 1,3-nitrogen shift

To a Schlenk tube was added the azanyl ester (1 equiv.), $K_2CO_3$ (3 equiv.) and (*R*,*R*)-[$FeCl_2$(**BIP**)] (8-15 mol%). 1,1,2,2-Tetrachloroethane (*c* 0.1 M) was added, and the mixture was degassed via freeze-pump-thaw for two times. The tube was sealed, and the reaction mixture was stirred at 0 °C for 40 hours or at room temperature (25 °C) for 16 hours. After completion, the reaction was quenched by a mixture of brine and hydrochloric acid, and subsequently extracted with EtOAc. The combined organic layer

was dried and was concentrated under reduced pressure, and the residue was purified by column chromatography on silica gel using a mixture of EtOAc and *n*-hexane (with 0.1% trifluoroacetic acid as the additive) to obtain the non-racemic α-amino acids **43**-**53**.

## Supplementary Material

Refer to Web version on PubMed Central for supplementary material.

## Acknowledgments

This project has received funding from the European Research Council (ERC) under the European Union's Horizon 2020 research and innovation programme (grant agreement No 883212). Funding was also provided by the Deutsche Forschungsgemeinschaft (Me 1805/15-1). S.C. thanks Oberlin College for financial support. DFT calculations were performed using the SCIURus, the Oberlin College HPC cluster (NSF MRI 1427949), and the startup allocations awarded by Extreme Science and Engineering Discovery Environment (XSEDE TG-CHE200100).

## Data availability

All relevant data supporting the findings of this study, including experimental procedures and compound characterization, NMR and HPLC are available within the Article and its Supplementary Information.

## References

1. Saghyan, AS, Langer, P. Asymmetric Synthesis of Non-Proteinogenic Amino Acids. Wiley-VCH; Weinheim: 2016.
2. Nájera C, Sansano JM. Catalytic asymmetric synthesis of α-amino acids. Chem Rev. 2007; 107: 4584–4671. [PubMed: 17915933]
3. Janey JM. Recent advances in catalytic, enantioselective α aminations and α oxygenations of carbonyl compounds. Angew Chem Int Ed. 2005; 44: 4292–4300.
4. Bøgevig A, Juhl K, Kumaragurubaran N, Zhuang W, Jørgensen KA. Direct organo-catalytic asymmetric α-amination of aldehydes—a simple approach to optically active α-amino aldehydes, α-amino alcohols, and α-amino acids. Angew Chem Int Ed. 2002; 41: 1790–1793.
5. List B. Direct catalytic asymmetric α-amination of aldehydes. J Am Chem Soc. 2002; 124: 5656–5657. [PubMed: 12010036]
6. Kumaragurubaran N, Juhl K, Zhuang W, Bøgevig A, Jørgensen KA. Direct L-proline-catalyzed asymmetric α-amination of ketones. J Am Chem Soc. 2002; 124: 6254–6255. [PubMed: 12033850]
7. Morrill LC, Lebl T, Slawin AMZ, Smith AD. Catalytic asymmetric α-amination of carboxylic acids using isothioureas. Chem Sci. 2012; 3: 2088–2093.
8. Dequirez G, Pons V, Dauban P. Nitrene chemistry in organic synthesis: still in its infancy? Angew Chem Int Ed. 2012; 51: 7384–7395.
9. Park Y, Kim Y, Chang S. Transition metal-catalyzed C−H amination: scope, mechanism, and applications. Chem Rev. 2017; 117: 9247–9301. [PubMed: 28051855]
10. Ju M, Schomaker JM. Nitrene transfer catalysts for enantioselective C−N bond formation. Nat Rev Chem. 2021; 5: 580–594.
11. Nägeli I, Baud C, Bernardinelli G, Jacquier Y, Moraon M, Müllet P. Rhodium(II)-catalyzed CH insertions with {[(4-nitrophenyl)sulfonyl]imino}phenyl-$\lambda^3$-iodane. Helv Chim Acta. 1997; 80: 1087–1105.
12. Zhou X-G, Yu X-Q, Huang J-S, Che C-M. Asymmetric amidation of saturated C−H bonds catalysed by chiral ruthenium and manganese porphyrins. Chem Commun. 1999. 2377–2378.
13. Kohmura Y, Katsuki T. Mn(salen)-catalyzed enantioselective C−H amination. Tetrahedron Lett. 2001; 42: 3339–3342.

14. Yamawaki M, Tsutsui H, Kitagaki S, Anada M, Hashimoto S. Dirhodium(II) tetrakis[N-tetrachlorophthaloyl-(*S*)-*tert*-leucinate]: a new chiral Rh(II) catalyst for enantioselective amidation of C−H bonds. Tetrahedron Lett. 2002; 43: 9561–9564.
15. Liang C, Robert-Peillard F, Fruit C, Müller P, Dodd RH, Dauban P. Efficient diastereoselective intermolecular rhodium-catalyzed C−H amination. Angew Chem Int Ed. 2006; 45: 4641–4644.
16. Nishioka Y, Uchida T, Katsuki T. Enantio- and regioselective intermolecular benzylic and allylic C−H bond amination. Angew Chem Int Ed. 2013; 52: 1739–1742.
17. Höke T, Herdtweck E, Bach T. Hydrogen-bond mediated regio- and enantioselectivity in a C−H amination reaction catalysed by a supramolecular Rh(II) complex. Chem Commun. 2013; 49: 8009–8011.
18. Nasrallah A, Boquet V, Hecker A, Retailleau P, Darses B, Dauban P. Catalytic enantioselective intermolecular benzylic C($sp^3$)−H amination. Angew Chem Int Ed. 2019; 58: 8192–8196.
19. Jin L-M, Xu P, Xie J, Zhang XP. Enantioselective intermolecular radical C−H amination. J Am Chem Soc. 2020; 142: 20828–20836. [PubMed: 33238707]
20. Liang J-L, Yuan S-X, Huang J-S, Yu W-Y, Che C-M. Highly diastereo- and enantioselective intramolecular amidation of saturated C−H bonds catalyzed by ruthenium porphyrins. Angew Chem Int Ed. 2002; 41: 3465–3468.
21. Milczek E, Boudet N, Blakey S. Enantioselective C−H amination using cationic ruthenium(II) −pybox catalysts. Angew Chem Int Ed. 2008; 47: 6825–6828.
22. Ichinose M, Suematsu H, Yasutomi Y, Nishioka Y, Uchida T, Katsuki T. Enantioselective intramolecular benzylic C−H bond amination: efficient synthesis of optically active benzosultams. Angew Chem Int Ed. 2011; 50: 9884–9887.
23. Zalatan DN, Du Bois J. A chiral rhodium carboxamidate catalyst for enantioselective C−H amination. J Am Chem Soc. 2008; 130: 9220–9221. [PubMed: 18582043]
24. Lang K, Torker S, Wojtas L, Zhang XP. Asymmetric induction and enantiodivergence in catalytic radical C−H amination via enantiodifferentiative H-atom abstraction and stereoretentive radical substitution. J Am Chem Soc. 2019; 141: 12388–12396. [PubMed: 31280562]
25. Park Y, Chang S. Asymmetric formation of γ-lactams via C−H amidation enabled by chiral hydrogen-bond-donor catalysts. Nat Catal. 2019; 9: 219–227.
26. van Vliet KM, de Bruin B. Dioxazolones: stable substrates for the catalytic transfer of acyl nitrenes. ACS Catal. 2020; 10: 4751–4769.
27. Zheng Y, Tan Y, Harms K, Marsch M, Riedel R, Zhang L, Meggers E. Octahedral ruthenium complex with exclusive metal-centered chirality for highly effective asymmetric catalysis. J Am Chem Soc. 2017; 139: 4322–4325. [PubMed: 28290685]
28. Zhou Z, Chen S, Qin J, Nie X, Zheng X, Harms K, Riedel R, Houk KN, Meggers E. Catalytic enantioselective intramolecular C($sp^3$)−H amination of 2-azidoacetamides. Angew Chem Int Ed. 2019; 58: 1088–1093.
29. Zhou Z, Tan Y, Yamahira T, Ivlev S, Xie X, Riedel R, Hemming M, Kimura M, Meggers E. Enantioselective ring-closing C−H amination of urea derivatives. Chem. 2020; 6: 2024–2034.
30. Thirumurugan P, Matosiuk D, Jozwiak K. Click chemistry for drug development and diverse chemical−biology applications. Chem Rev. 2013; 113: 4905–4979. [PubMed: 23531040]
31. Ueno K, Kubo S, Tagawa H, Yoshioka T, Tsukada W, Tsubokawa M, Kojima H, Kasahara A. 6,11-Dihydro-11-oxodibenz[*b*,*e*]oxepinacetic acids with potent antiinflammatory activity. J Med Chem. 1976; 19: 941–946. [PubMed: 940112]
32. Krupp PJ, Menassé-Gdynia R, Sallmann A, Wilhelmi G, Ziel R, Jaques R. Sodium [*o*-[(2,6-dichlorophenyl)-amino]-phenyl]-acetate (GP 45 840), a new non-steroidal anti-inflammatory agent. Experientia. 1973; 29: 450–452. [PubMed: 4708344]
33. Bauer I, Knölker H-J. Iron catalysis in organic synthesis. Chem Rev. 2015; 115: 3170–3387. [PubMed: 25751710]
34. Liu Y, You T, Wang H-X, Tang Z, Zhou C-Y, Che C-M. Iron- and cobalt-catalyzed C($sp^3$)−H bond functionalization reactions and their application in organic synthesis. Chem Soc Rev. 2020; 49: 5310–5358. [PubMed: 32568340]

35. Hong Y, Jarrige L, Harms K, Meggers E. Chiral-at-iron catalyst: expanding the chemical space for asymmetric earth-abundant metal catalysis. J Am Chem Soc. 2019; 141: 4569–4572. [PubMed: 30839201]
36. Chen MS, White MC. A predictably selective aliphatic C−H oxidation reaction for complex molecule synthesis. Science. 2007; 318: 783–787. [PubMed: 17975062]
37. Gormisky PE, White MC. Catalyst-controlled aliphatic C−H oxidations with a predictive model for site-selectivity. J Am Chem Soc. 2013; 135: 14052–14055. [PubMed: 24020940]
38. Mitra M, Cusso O, Bhat SS, Sun M, Cianfanelli M, Costas M, Nordlander E. Highly enantioselective epoxidation of olefins by H2O2 catalyzed by a non-heme Fe(II) catalyst of a chiral tetradentate ligand. Dalton Trans. 2019; 48: 6123–6131. [PubMed: 30951054]
39. Poli R, Harvey JN. Spin forbidden chemical reactions of transition metal compounds. New ideas and new computational challenges. Chem Soc Rev. 2003; 32: 1–8. [PubMed: 12596540]
40. Harvey JN, Poli R, Smith KM. Understanding the reactivity of transition metal complexes involving multiple spin states. Coord Chem Rev. 2003; 238–239: 347–361.
41. Yersin H, Humbs W. Spatial extensions of excited states of metal complexes. Tunability by chemical variation. Inorg Chem. 1999; 38: 5820–5831.
42. Maestre L, Sameera WMC, Díaz-Requejo MM, Maseras F, Pérez PJ. A general mechanism for the copper- and silver-catalyzed olefin aziridination reactions: concomitant involvement of the singlet and triplet pathways. J Am Chem Soc. 2013; 135: 1338–1348. [PubMed: 23276287]
43. Jung H, Keum H, Kweon J, Chang S. Tuning triplet energy transfer of hydroxamates as the nitrene precursor for intramolecular C($sp^3$)−H amidation. J Am Chem Soc. 2020; 142: 5811–5818. [PubMed: 32129618]
44. Ess DH, Houk KN. Theory of 1,3-dipolar cycloadditions: distortion/interaction and frontier molecular orbital models. J Am Chem Soc. 2008; 130: 10187–10198. [PubMed: 18613669]
45. Krenske EH, Houk KN. Aromatic interactions as control elements in stereoselective organic reactions. Acc Chem Res. 2013; 46: 979–989. [PubMed: 22827883]
46. Wheeler SE. Understanding substituent effects in noncovalent interactions involving aromatic rings. Acc Chem Res. 2013; 46: 1029–1038. [PubMed: 22725832]
47. Wheeler SE, Bloom JWG. Toward a more complete understanding of noncovalent interactions involving aromatic rings. J Phys Chem A. 2014; 118: 6133–6147. [PubMed: 24937084]
48. Isidro-Llobet A, Álvarez M, Albericio F. Amino acid-protecting groups. Chem Rev. 2009; 109: 2455–2504. [PubMed: 19364121]
49. Blaskovich MAT. Unusual amino acids in medicinal chemistry. J Med Chem. 2016; 59: 10807–10836. [PubMed: 27589349]
50. Agostini F, Völler J-S, Koksch B, Acevedo-Rocha CG, Kubyshkin V, Budisa N. Biocatalysis with unnatural amino acids: enzymology meets xenobiology. Angew Chem Int Ed. 2017; 56: 9680–9703.
51. Drienovská I, Roelfes G. Expanding the enzyme universe with genetically encoded unnatural amino acids. Nat Catal. 2020; 3: 193–202.

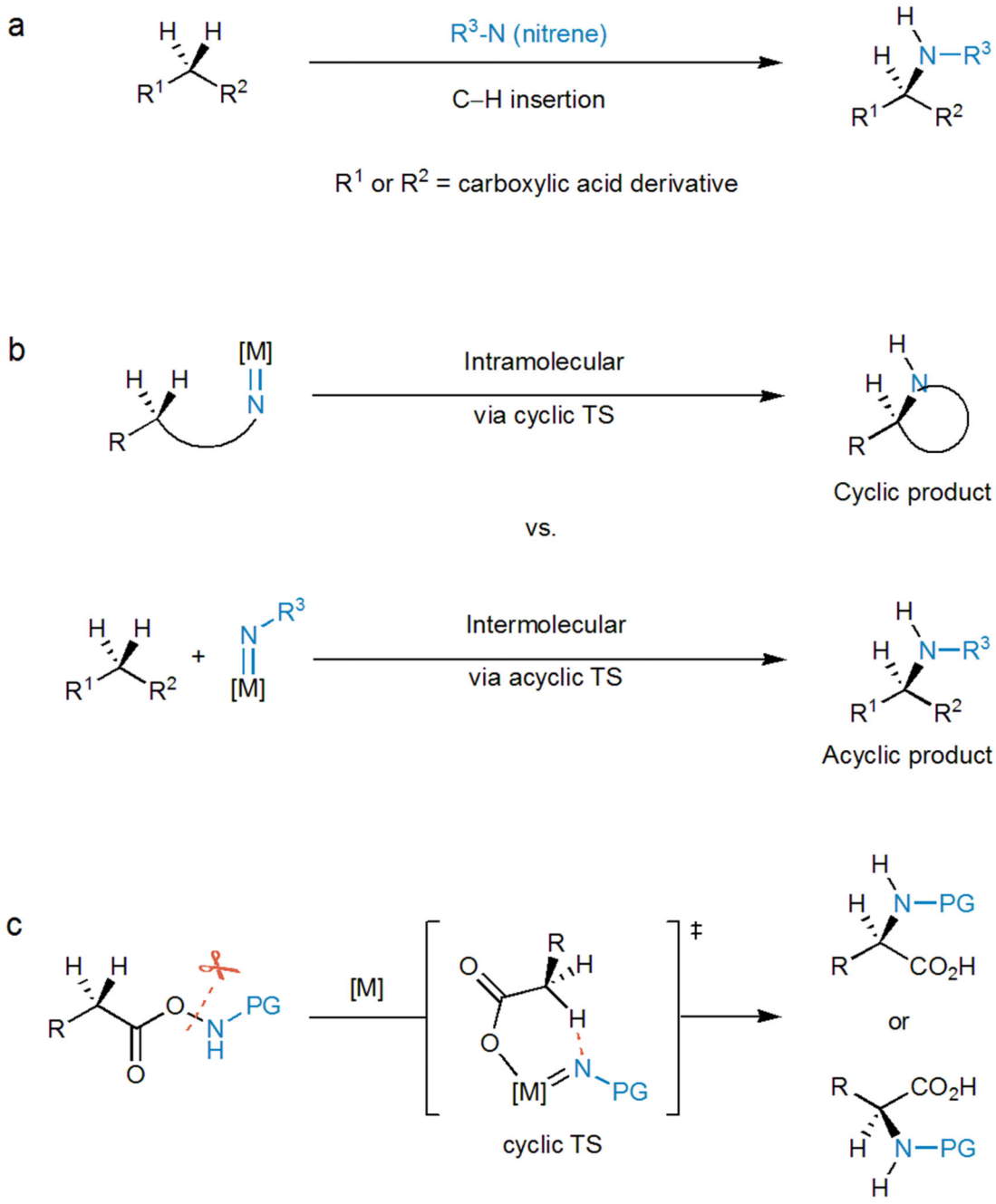


**Fig. 1. Stereocontrolled nitrene C($sp^3$)−H insertions for the synthesis of α-amino acids.**

**a**, Strategy for the straightforward synthesis of α-amino acids by nitrene C−H insertion. **b**, Intramolecular nitrene C−H insertion goes via a cyclic transition state to form a cyclic product, while intermolecular nitrene C−H insertion forms acyclic products. **c**, Proposed 1,3-nitrogen migration which combines the advantages of intramolecular (high regio- and stereocontrol via cyclic TS) and intermolecular (acyclic product formation) C−H insertion chemistry. TS = transition state, PG = protecting group.

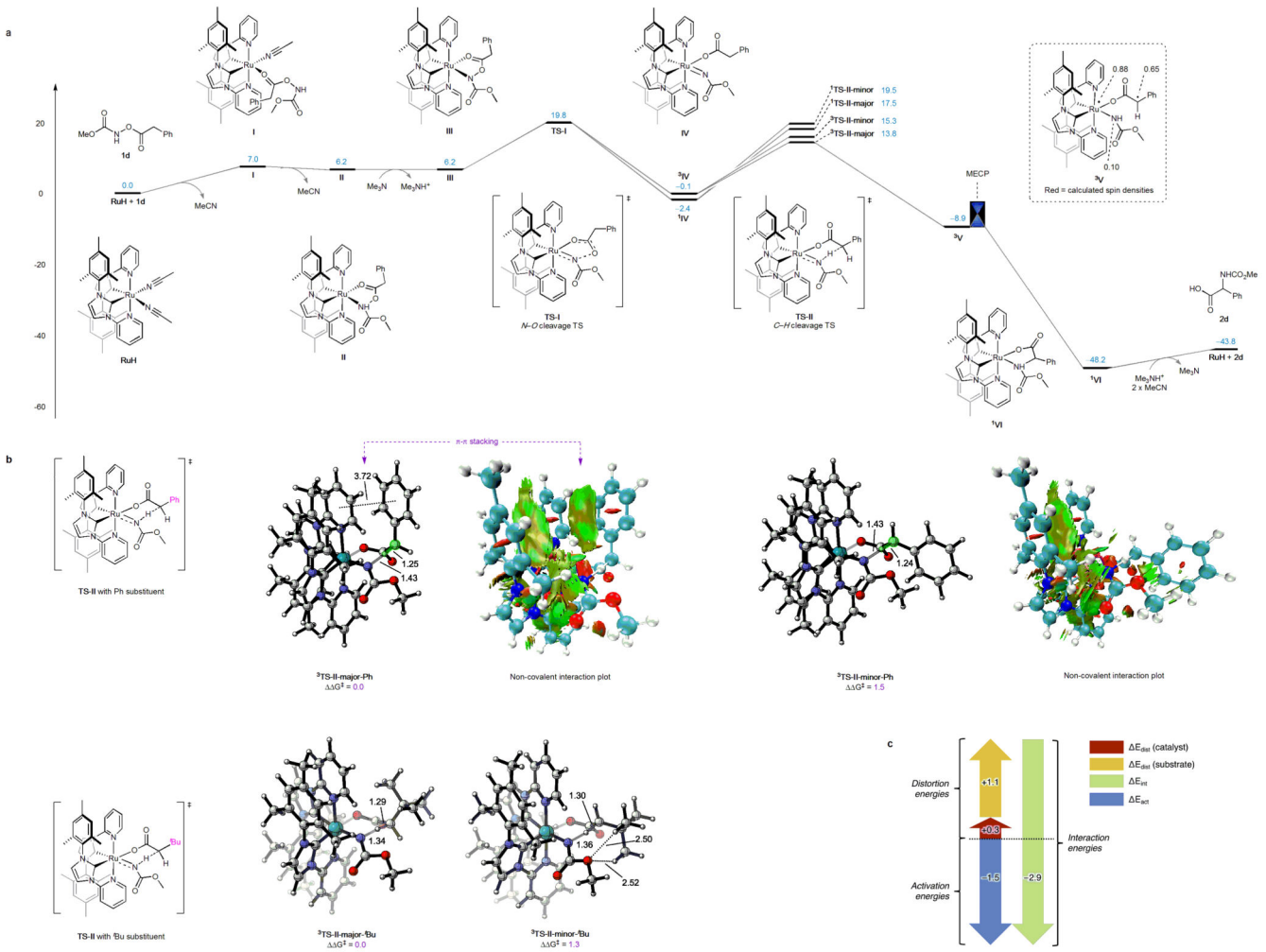


**Fig. 2. Investigation of the reaction mechanism.**

**a**, Calculated free-energy profile for the 1,3-nitrogen migration of model substrate **1d** with **RuH** as the catalyst (energies provided in kcal/mol). Ruthenium catalyzes the cleavage of the N−O bond of **1d** via transition state **TS-I** leading to the carboxylate coordinated ruthenium nitrene intermediate **IV**. This is followed by singlet-triplet spin crossover to the triplet state of **IV** followed by an exergonic hydrogen atom transfer via cyclic transition state **TS-II** to generate diradical intermediate **V** in its triplet state. Next, C−N bond formation occurs upon spin crossover to the singlet state through a minimum energy crossing point (MECP) to generate the chelate complex **VI**. Protonation of the coordinated carboxylate moiety finally releases the product **2d**. **b**, Geometries and non-covalent interaction plots of calculated transition states for the hydrogen atom transfer step to provide insight into the origin of stereodiscrimination (interatomic distances provided in ångströms). The results reveal that in **$^3$TS-II-major-Ph**, a favorable **π−π** stacking interaction exists between the ligand framework of the catalyst and the phenyl substituent of the substrate **1d** (**TS-II** with Ph substituent). This favorable **π−π** stacking interaction is absent from **$^3$TS-II-minor-Ph**. The calculations also confirm that stereodiscrimination can be achieved with a substrate bearing a $^t$Bu instead of a Ph side chain (**TS-II** with $^t$Bu substituent). **c**,




Europe PMC Funders Author Manuscripts

Distortion-interaction analysis performed on $^{3}$TS-II-major-Ph and $^{3}$TS- II-minor-Ph. The more favorable interaction energy in $^{3}$TS-II-major-Ph further supports the contribution of stabilizing interactions such as π−π stacking to the stereoselectivity in the formation of phenyl glycine derivative **2d**.



Europe PMC Funders Author Manuscripts

Europe PMC Funders Author Manuscripts

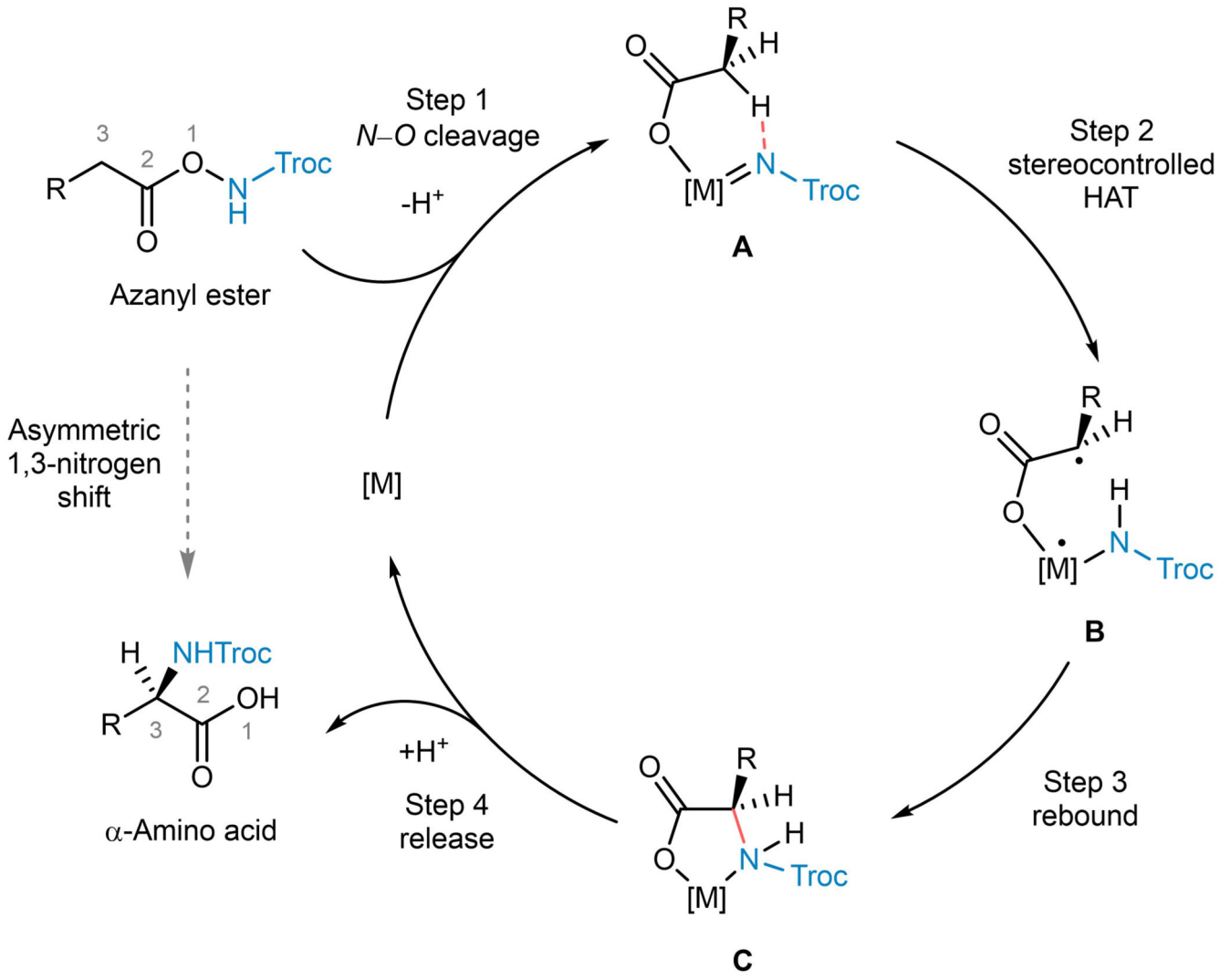


**Fig. 3. Summary of proposed simplified mechanism.**

The catalytic cycle of the asymmetric 1,3-nitrogen migration commences with N−O cleavage of azanyl ester in presence of metal catalyst, proceeds through stereocontrolled hydrogen atom transfer and subsequent rebound of the diradical, and concludes with release of the α-amino acid and catalyst regeneration.

Europe PMC Funders Author Manuscripts

**Table 1**

**Initial experiments and optimization of enantioselective 1,3-nitrogen shift**

Europe PMC Funders Author Manuscripts

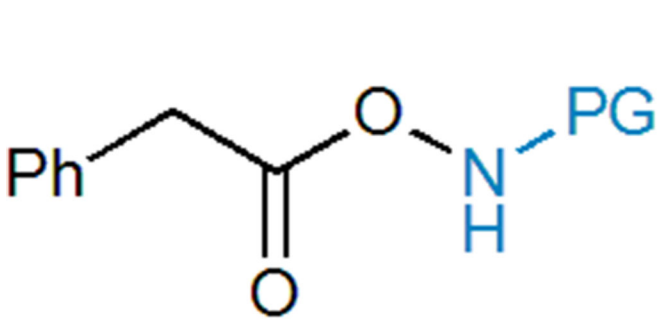


**Ru cat.** (1 mol
$K_2CO_3$ (3 equi

$CH_2Cl_2$, r.t., 16
standard condit

**1a-e**

PG =

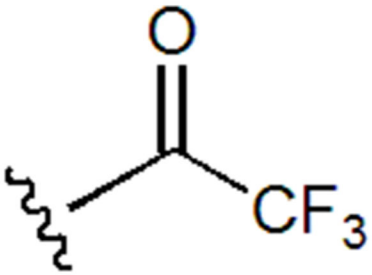


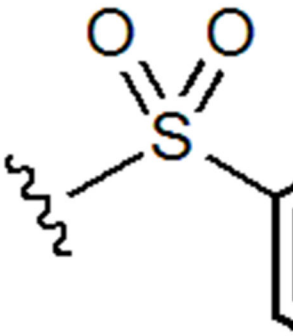




**a** **b**

| Entry | Catalyst | Protectin |
|---|---|---|
| 1 | A, R=PMP | COCF3 (a |

Europe PMC Funders Author Manuscripts

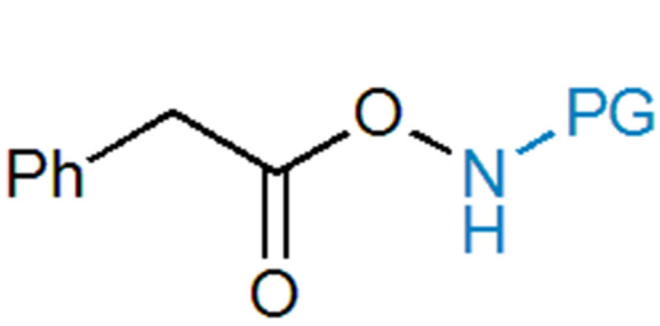


**Ru cat.** (1 mol
$K_2CO_3$ (3 equi

$CH_2Cl_2$, r.t., 16
standard condit

**1a-e**

PG =

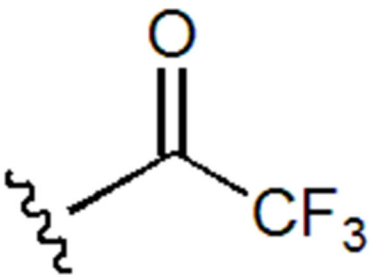


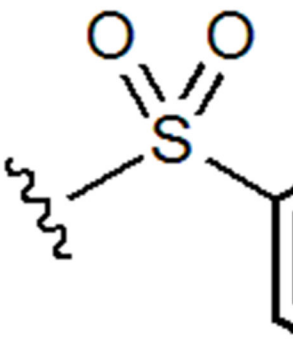




**a** **b**

| Entry | Catalyst | Protectin |
|---|---|---|
| 2 | Λ-**RuDMP** | Ts(b) |

Europe PMC Funders Author Manuscripts

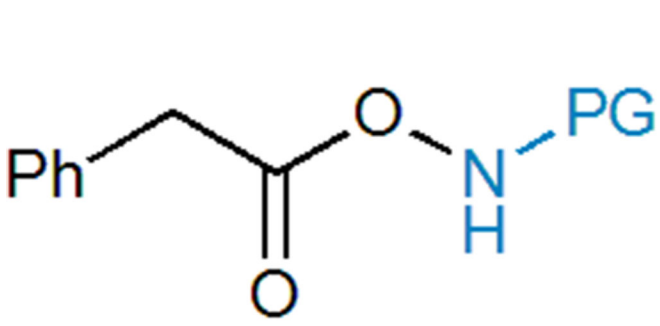


**1a-e**

**Ru cat.** (1 mol
$K_2CO_3$ (3 equi
$CH_2Cl_2$, r.t., 16
standard condit

PG =

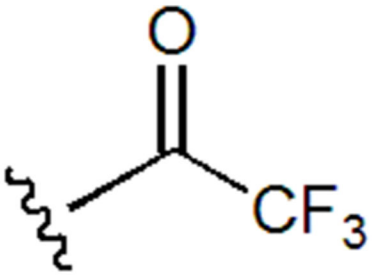


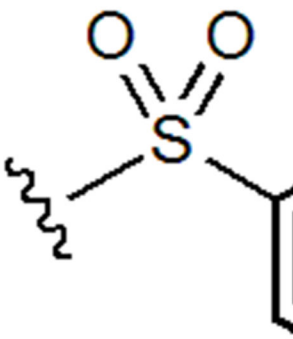




**a** **b**

| Entry | Catalyst | Protectin |
|---|---|---|
| 3 | Λ-**RuDMP** | Ms (c) |

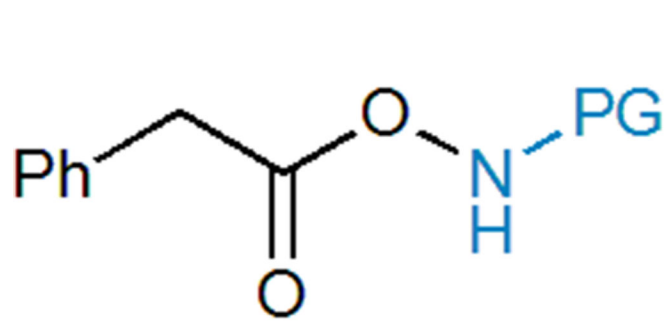


**Ru cat.** (1 mol
$K_2CO_3$ (3 equi

$CH_2Cl_2$, r.t., 16
standard condit

**1a-e**

PG =

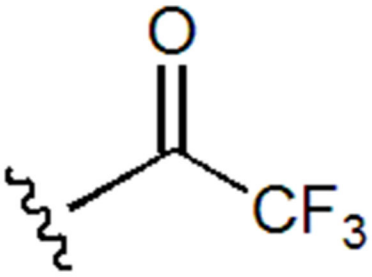


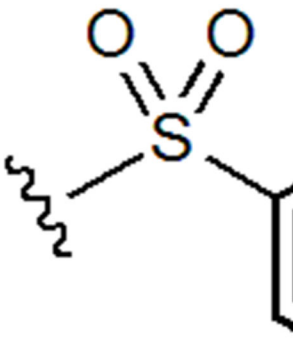


*Nat Chem*. Author manuscript; available in PMC 2022 October 04.

**a** **b**

| Entry | Catalyst | Protectin |
|---|---|---|
| 4 | Λ-**RuDMP** | $CO_2Me$ (c |

Europe PMC Funders Author Manuscripts

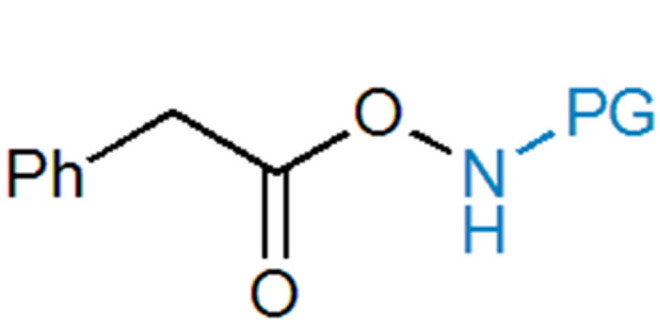


**Ru cat.** (1 mol
$K_2CO_3$ (3 equi

$CH_2Cl_2$, r.t., 16
standard condit

**1a-e**

PG =

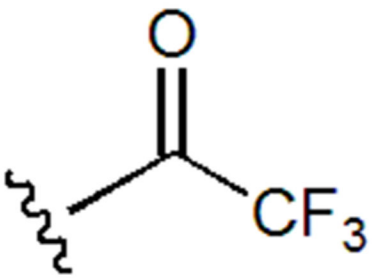


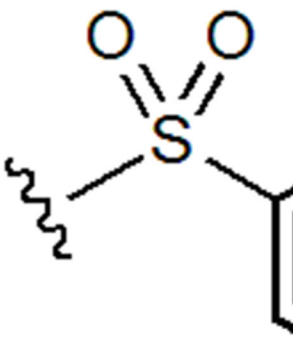


*Nat Chem*. Author manuscript; available in PMC 2022 October 04.

**a** **b**

| Entry | Catalyst | Protectin |
|---|---|---|
| 5 | Λ-**RuDMP** | Troc (e) |

Europe PMC Funders Author Manuscripts

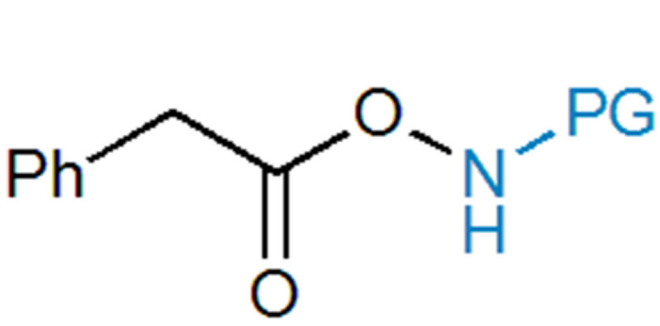


**Ru cat.** (1 mo
$K_2CO_3$ (3 equi
$CH_2Cl_2$, r.t., 1
standard condit

**1a-e**

PG =

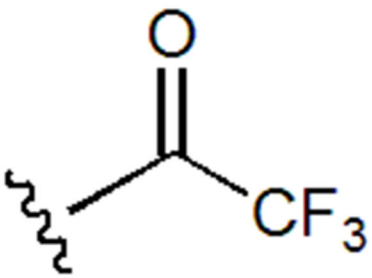


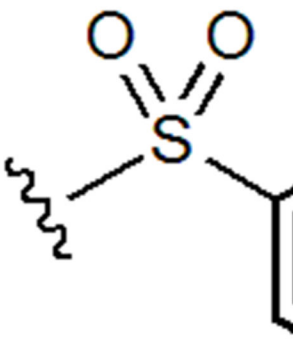




**a** **b**

| Entry | Catalyst | Protectin |
|---|---|---|
| 6 | Λ-**RuTMS** | Troc (e) |

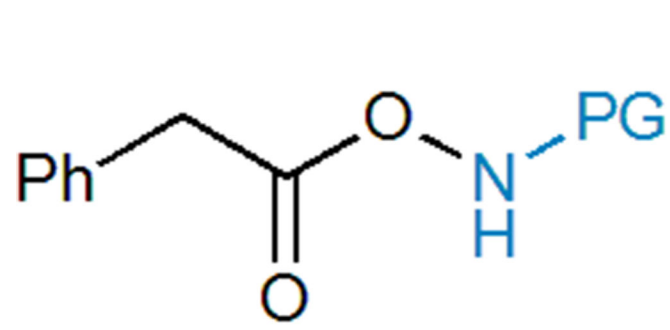


**1a-e**

**Ru cat.** (1 mol
$K_2CO_3$ (3 equi
$CH_2Cl_2$, r.t., 16
standard condit

PG =

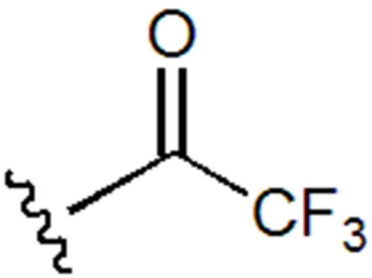


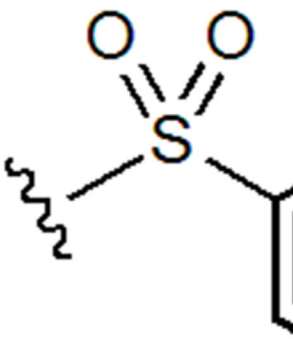


*Nat Chem*. Author manuscript; available in PMC 2022 October 04.

**a** **b**

| Entry | Catalyst | Protectin |
|---|---|---|
| 7 | Λ-**RuCF**$_3$ | Troc (e) |

Europe PMC Funders Author Manuscripts

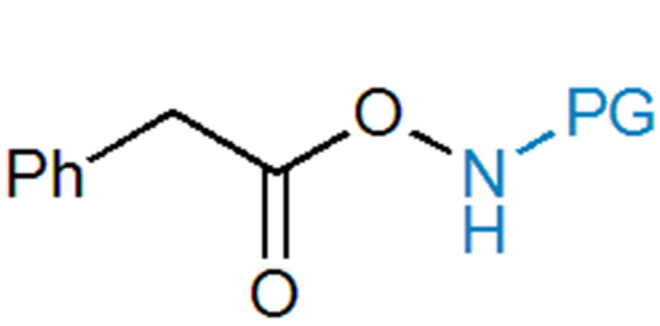


**Ru cat.** (1 mol
$K_2CO_3$ (3 equi
$CH_2Cl_2$, r.t., 16
standard condit

**1a-e**

PG =

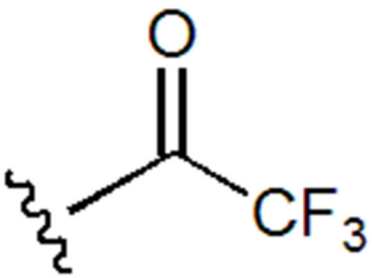


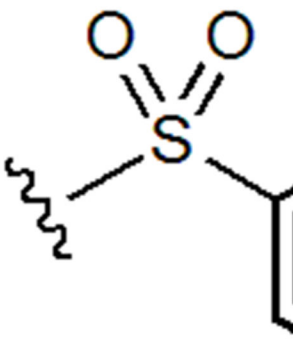


*Nat Chem*. Author manuscript; available in PMC 2022 October 04.

**a** **b**

| Entry | Catalyst | Protectin |
|---|---|---|
| 8 | Λ-**RuH** | Troc (e) |

Europe PMC Funders Author Manuscripts



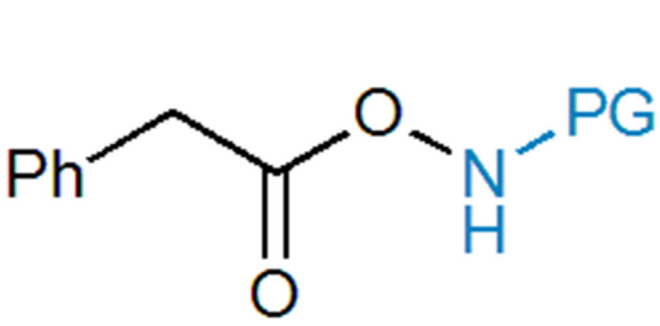


**Ru cat.** (1 mol
$K_2CO_3$ (3 equi
$CH_2Cl_2$, r.t., 16
standard condit

**1a-e**

PG =

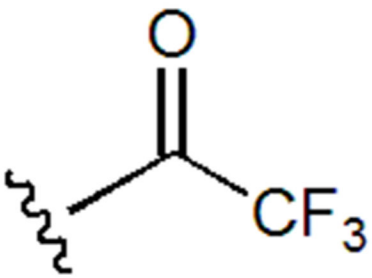


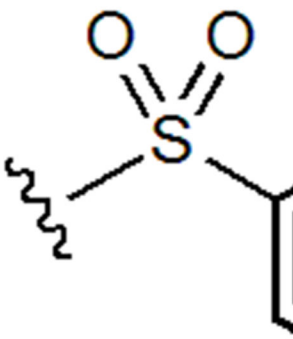


*Nat Chem*. Author manuscript; available in PMC 2022 October 04.

**a** **b**

| Entry | Catalyst | Protectin |
|---|---|---|
| 9 | Λ-**RuDMP** | Troc (e) |

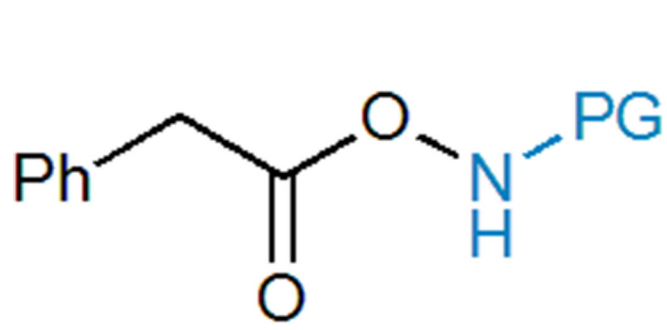


**Ru cat.** (1 mol
$K_2CO_3$ (3 equi
$CH_2Cl_2$, r.t., 16
standard condit

**1a-e**

PG =

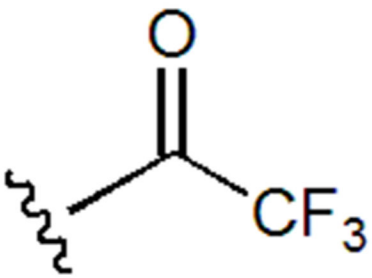


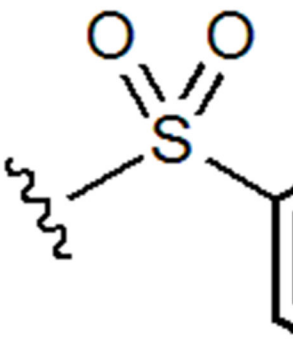


*Nat Chem*. Author manuscript; available in PMC 2022 October 04.

**a** **b**

| Entry | Catalyst | Protectin |
|---|---|---|
| 10 | Λ-**RuDMP** | Troc (e) |

Europe PMC Funders Author Manuscripts

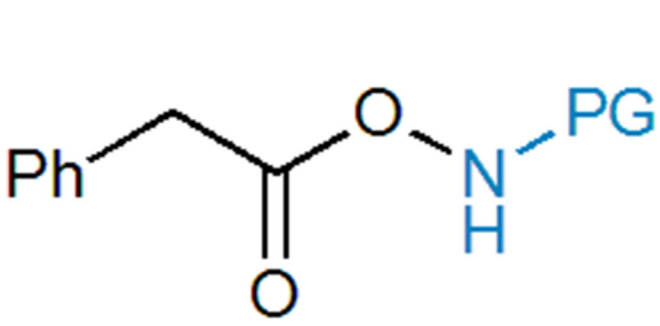


**1a-e**

**Ru cat.** (1 mol
$K_2CO_3$ (3 equi
$CH_2Cl_2$, r.t., 16
standard condit

PG =

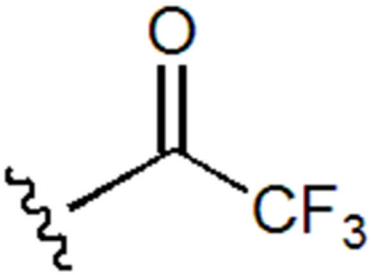


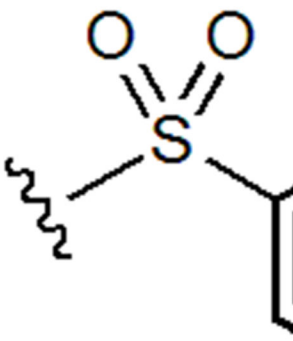




**a** **b**

| Entry | Catalyst | Protectin |
|---|---|---|
| 11 | Λ-**RuDMP** | Troc (e) |

Europe PMC Funders Author Manuscripts

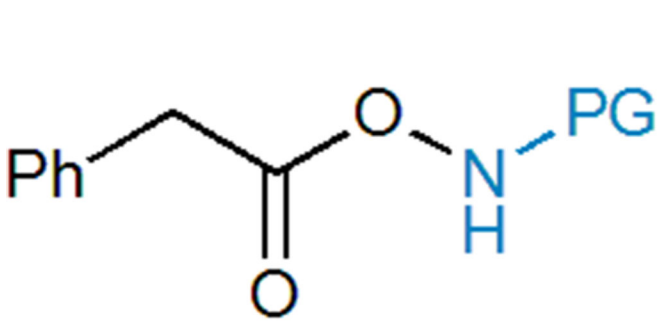


**Ru cat.** (1 mol
$K_2CO_3$ (3 equi

$CH_2Cl_2$, r.t., 16
standard condit

**1a-e**

PG =

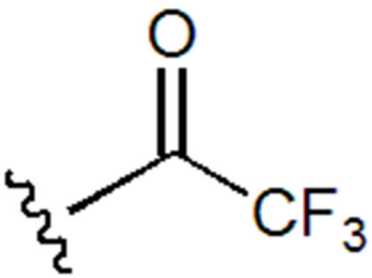


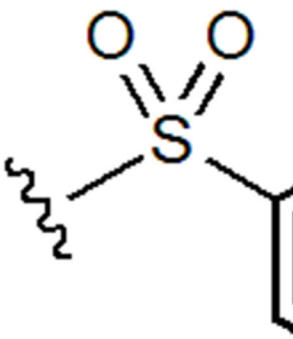


*Nat Chem*. Author manuscript; available in PMC 2022 October 04.

**a** **b**

| Entry | Catalyst | Protectin |
|---|---|---|
| 12 | Λ-**RuDMP** | Troc (e) |

[a] Shown are the deviations from the standard reaction conditions. Standard conditions: substrate 1 (0.1 mmol), Ru catalyst (1 mol%) and the indicated base (3 equiv.) in the indicated solvent (2 mL, c 0.05 M) were stirred at room temperature (25 °C) for 16 hours.

[b] Conversion and yield were determined by $^{1}$H NMR analysis using hexamethylbenzene as an internal standard.

[c] Enantiomeric excess (e.e.) values were determined by HPLC on chiral stationary phases.

[d] Yield of the isolated α-amino acid. n.d. = not determined. Troc = $CO_2CH_2CCl_3$.



Europe PMC Funders Author Manuscripts

## Table 2

### Substrate scope for ruthenium catalysis

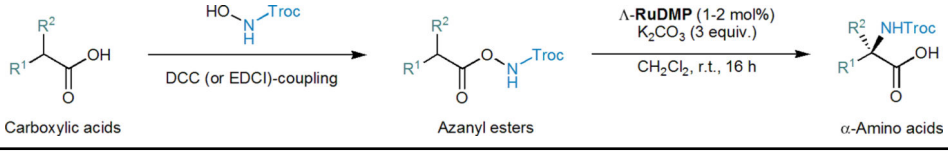


α-Aryl amino acids

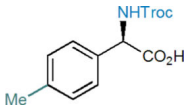

**3**
86%, 97% e.e.

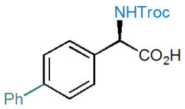

**4**
86%, 95% e.e.

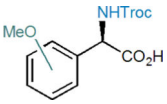

**5**(para), 96%, 96% e.e.
**6**(*meta*), 87%, 96% e.e.
**7**(*ortho*), 79%, 85% e.e.

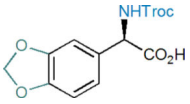

**8**
56%, 92% e.e.

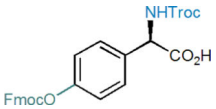

**9**
83%, 93% e.e.

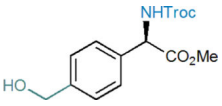

**10**[a]
64%, 98% e.e.

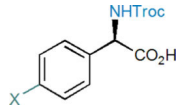

**11**, X = I, 91%, 94% e.e.
**12**, X = Br, 93%, 94% e.e.
**13**, X = Cl, 93%, 95% e.e.
**14**, X = F, 92%, 93% e.e.

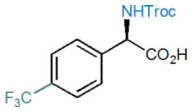

**15**
87%, 86% e.e.

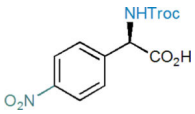

**16**
73%, 92% e.e.

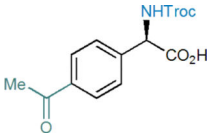

**17**
79%, 92% e.e.

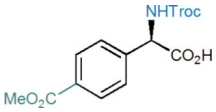

**18**
91%, 93% e.e.

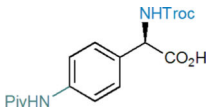

**19**
93%, 96% e.e.

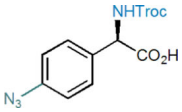

**20**
95%, 97% e.e.

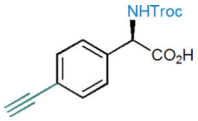

**21**
88%, 94% e.e.

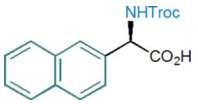

**22**
92%, 96% e.e.

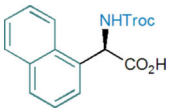

**23**[b]
92%, 95% e.e.

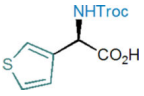

**24**
84%, 95% e.e.

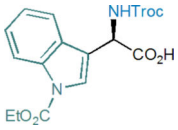

**25**
77%, 90% e.e.

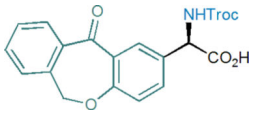

**26**(87%, 98% e.e.)
from isoxepac

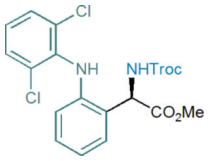

**27**[a] (54%, 96% e.e.)
from diclofenac

α-Alkenyl, α-alkynyl & α-alkyl amino acids

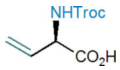

**28**
62%, 73% e.e.

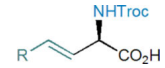

**29**, R = Et, 83%, 84% e.e.
**30**, R = ‘Pr, 88%, 81% e.e.
**31**, R = [n]Hex, 85%, 82% e.e.
**32**, R = Ph, 88%, 82% e.e.

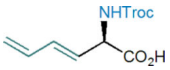

**33**
72%, 81% e.e.

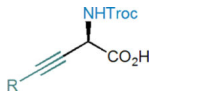

**34**[c], R = Ph, 46%, 62% e.e.
**35**[c], R = Et, 63%, 64% e.e.

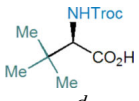

**36**[d]
20%, 90% e.e.

α-Disubstituted amino acids (stereoretentive 1,3-nitrogen shift)

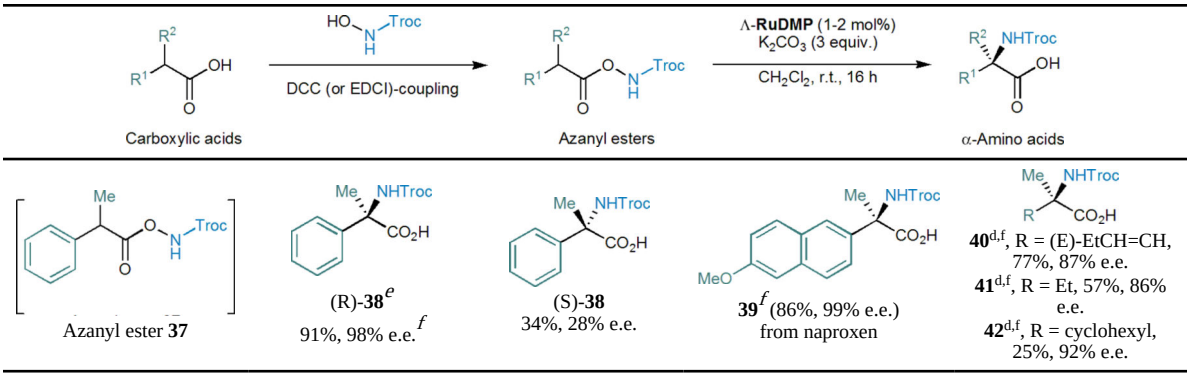


Conditions for enantioselective 1,3-nitrogen shift: reactions were carried out with Λ-**RuDMP** (1-2 mol%), $K_2CO_3$ (3 equiv.) and $CH_2Cl_2$ (c 0.05 M) at room temperature (25 °C) for 16 h. Enantiomeric excess (e.e.) values were determined by HPLC analysis (see Supplementary Information section 4 for full details).

[a] Isolated after conversion to the methyl ester.

[b] Additional gram-scale reaction performed with 3.5 mmol (1.32 gram) azanyl ester gave **23** in 91% yield with 95% e.e. (see Supplementary Information section 6 for full details).

[c] $KHCO_3$ instead of $K_2CO_3$ as a base.

[d] Λ-RuH (2-10 mol%) as the catalyst.

[e] The reaction performed with racemic azanyl ester **37** afforded (*R*)-**38** in 71% yield with 48% e.e.

[f] Reaction performed with enantiopure (*S*)-azanyl ester.

[g] Reaction performed with enantiopure (*R*)(*S*)-**38**-azanyl ester.




Europe PMC Funders Author Manuscripts

## Table 3

### Substrate scope for iron catalysis

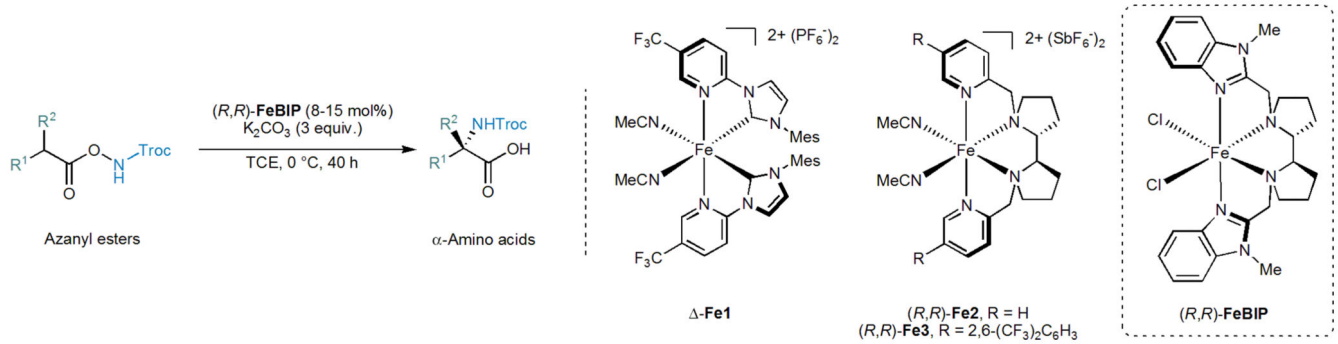


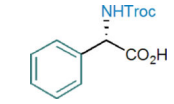

(S)-**2e**
Δ-**Fe1** (8 mol%), trace
(R,R)-**Fe2** (8 mol%), 91%, 15% e.e.
(R,R)-**Fe3** (8 mol%), 75%, 10% e.e.
(R,R)-**FeBIP** (8 mol%), 95%, 91% e.e.

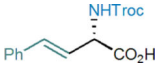

(S)-**32**
44%, 86% e.e.

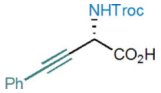

(S)-**34**
13%, 44% e.e.

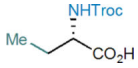

**43**
62%, 91% e.e.

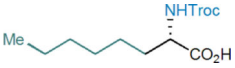

**44**
75%, 92% e.e.

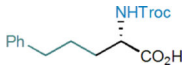

**45**
60%, 91% e.e.

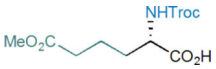

**46**
70%, 90% e.e.

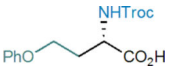

**47**
53%, 90% e.e.

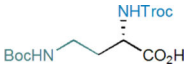

**48**[a,b]
51%, 90% e.e.

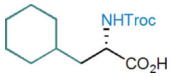

**49**
57%, 91% e.e.

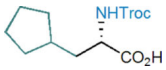

**50**
65%, 92% e.e.

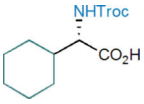

**51**
48%, 89% e.e.

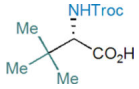

(S)-**36**
56%, 85% e.e.

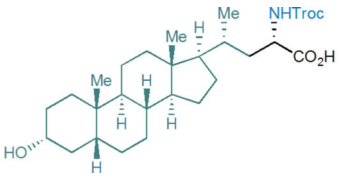

**52**[a] (77%, 23:1 d.r.)
from lithocholic acid

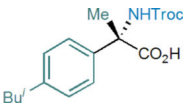

**53** (70%, 85% e.e.)
from (±)-ibuprofen

Reaction conditions: reactions were carried out with (*R,R*)-FeBIP (8-15 mol%), $K_2CO_3$ (3 equiv.) and 1,1,2,2-tetrachloroethane (TCE, *c* 0.1 M) at 0 °C for 40 h. Enantiomeric excess (e.e.) values were determined by HPLC analysis (see Supplementary Information section 4 for full details).

[a]Reaction performed at room temperature (25 °C) for 16 h.

[b]Isolated after conversion to the methyl ester.